Journal of Magnetic Resonance 198 (2009) 88–93

Contents lists available at ScienceDirect

Journal of Magnetic Resonance

journal homepage: www.elsevier.com/locate/jmr

Visualization of inhomogeneous local magnetic field gradient due to susceptibility contrast

H. Cho [a,b], S. Ryu [b], J.L. Ackerman [c], Y.-Q. Song [b,*]

[a] Memorial Sloan Kettering Cancer Center, 1275 York Avenue, New York, NY 10021, USA
[b] Schlumberger-Doll Research, One Hampshire Street, Cambridge, MA 02139, USA
[c] The Athinoula A. Martinos Center for Biomedical Imaging, Massachusetts General Hospital, 149 13th street, Charlestown, MA 02129, USA

ARTICLE INFO

Article history:
Received 24 June 2008
Revised 20 January 2009
Available online 23 February 2009

Keywords:
Internal magnetic field
Background gradient
Porous media

ABSTRACT

We visualized inhomogeneous local magnetic field (internal magnetic field) gradients arising from susceptibility contrast between an array of cylindrical glass tubes (solid matrix) and surrounding water (pore fluids) in a uniform applied magnetic field. MRI was performed to determine the spatially resolved decay rates due to diffusion in the internal magnetic field which were proportional to the strength of local gradient. We also spatially resolved the interference pattern of the cross-terms between the internal and the applied field gradient in order to extract the orientation of the internal field gradient. These experimental results were found to be consistent with the theoretical calculations. This work demonstrates a simple yet representative case for visualizing the strength and orientation of the local susceptibility induced magnetic field gradients in porous media.

1. Introduction

Nuclear magnetic resonance (NMR) has been widely used as a non-destructive way to characterize porous media. Pore space properties, such as porosity, permeability and surface-to-volume ratio, can be determined via spin relaxation measurements [1–3], time-dependent diffusion coefficient $D(t)$, and diffusion propagator measurements [4–8].

When a porous material is placed in a uniform magnetic field, spatially varying fields ($\vec{B}^{\text{int}}(r)$) typically arise inside the pore space due to susceptibility contrasts ($\triangle\chi$) between the solid matrix and the surrounding fluid. Susceptibility contrast is present in many porous media of interest, such as fluid filled rocks, cements, granular media, colloids and trabecular bones. The presence of non-uniform internal fields often interferes with NMR relaxation and diffusion measurements. Much effort has gone into understanding the effect of the internal gradient (also called background gradient) on NMR response and designing pulse sequences to cope with its interference with the applied gradient [9–11,5,12–14]. Recently, the idea of utilizing internal gradients as a finger-print of pore geometry has been proposed and implemented in the laboratory [15–17].

Historically, Brown et al. first computed magnetic field distributions from a single magnetized grain and a random packing of grains and observed the effects of such distributions on the decay of NMR signals [18]. Detailed numerical evaluation of the internal field in a 2D pack of cylinders and 3D random pack of spheres has been reported [19,20]. NMR responses were numerically evaluated based on CT images for sandstone and carbonate rocks [21].

Susceptibility-induced contrast (T_2^*) in biologic systems is often used to obtain functional and structural information of underlying tissues, as in the BOLD effect [22] in functional MRI applications and the characterization of trabecular bone structure [23,24]. Hwang et al. applied MR phase mapping techniques to measure internal magnetic field in trabecular bone and showed good agreement with theoretical calculations based on surface charge method [23]. Sigmund et al. showed that DDIF contrast [15] from bone/fluid interface is sensitive to the projected surface to volume ratio of trabecular bone [24]. On the other hand, susceptibility induced magnetic field gradients are vector quantities, and the ability to obtain not only the strength/phase but the orientation information with MR method may provide unique opportunities to study the morphology of underlying tissues in more quantitative details. For example, T_2^* in lung tissue tends to be very short [25] and to exhibit a distribution of values [26] because of the air–tissue interface. Characterizing and understanding direction-dependent susceptibility effects could lead to improved lung imaging methods, as well as providing information on the microstructure of lung tissue [27]. Furthermore, capillary blood vessel geometry is known to be a significant determinant of susceptibility contrasts [28]. The ability to measure the directional dependence of susceptibility contrast in capillaries will provide useful information in quantifying microvascular tortuosity in tumor angiogenesis or in determining the preferential capillary direction in myocardial walls [29].

* Corresponding author. Fax: +1 617 768 2386.
E-mail address: ysong@slb.com (Y.-Q. Song).

1090-7807/$ - see front matter © 2009 Elsevier Inc. All rights reserved.
doi:10.1016/j.jmr.2009.01.024

In this paper, we utilized the decay of the magnetization due to spins diffusing in the internal magnetic field (DDIF) for the direct experimental visualization of the strength of internal gradients. We performed microimaging experiments on a vessel-mimicking phantom composed of uniform cylindrical capillary tubes. Interference patterns of the cross-terms between the internal and applied gradient were resolved along different pulsed field gradient (PFG) orientations permitting the extraction of the vector components of the internal gradient and thus allowing directional mapping of internal gradients. Excellent agreement with theoretical calculations was observed.

2. Method

The sample consisted of an array of glass capillary tubes (Fisherbrand) with an ID 1.15 mm and wall thickness 0.2 mm, packed into a 13-mm NMR tube. It was filled with water both inside and between capillaries. MRI experiments were performed in a horizontal 4.7-T magnet (Bruker Biospin, Billerica, MA) with a 30-G/cm gradient set and a homemade RF probe tuned to 200 MHz. The orientation of the applied field was along the y direction which was perpendicular to the cylindrical axis (z) of the glass tubes. The internal field gradient is only in x–y plane due to the symmetry of the sample and the field direction.

A slice-selective stimulated echo sequence with spin-warp imaging was employed, shown in Fig. 1. The two t_e periods function as the encoding and decoding periods of the internal field gradient and t_d was the diffusion time. The duration (t_p) of the slice selective $\pi/2$ pulse was 2 ms and the strength of the slice gradient (G_s) was 4 G/cm. Transverse spin magnetization after the first $\pi/2$ pulse develops a spatially dependent phase due to the internal gradients. At the end of the encoding period, the encoded transverse magnetization was flipped back into the longitudinal direction and the spins diffuse during the t_d period. The third $\pi/2$ pulse was applied to produce a stimulated echo for magnetization detection and imaging. The decay of the echo was measured at a series of t_d values. The effective decay rates of the echo signal can be written as

$$\frac{1}{T_{\text{eff}}} = \frac{1}{T_1} + \frac{1}{T_{\text{ext}}} + \frac{1}{T_{\text{int}}} = \frac{1}{T_b} + \gamma^2 t_e^2 D g_{\text{int}}^2, \tag{1}$$

where γ, D and g_{int} are the gyromagnetic ratio, diffusion constant and the internal field gradient, respectively. $1/T_{\text{ext}} = \gamma^2 D(t_p G_s/2)^2$ originates from the unbalanced slice gradient during the second RF pulse and can be estimated to be 0.3 s^{-1}. Bulk relaxation

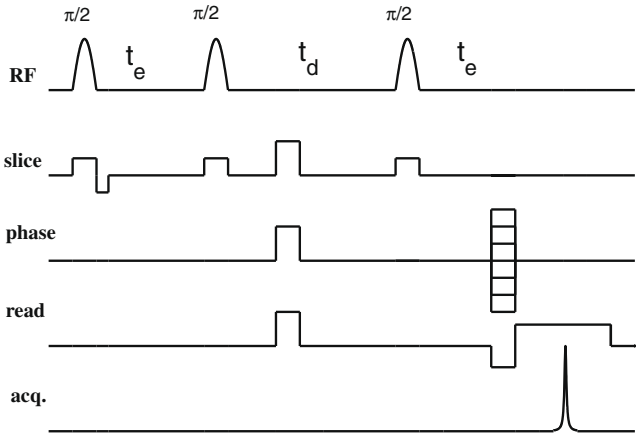

Fig. 1. Slice selective 2D spin-warp stimulated echo imaging sequence for DDIF contrast. The spoiler gradients were applied during t_d to remove unwanted coherence pathway signals other than the stimulated echo.

T_1 ($\sim 0.4\ s^{-1}$) also contributes to the effective signal decay. Therefore, there exists a total background decay rate $1/T_b$ of $\sim 0.7\ s^{-1}$ in addition to the decay due to internal field gradients ($1/T_{\text{int}}$).

The encoding time (t_e) was 0.040 s and the diffusion time (t_d) was varied from 0.05 to 1.1 s. Imaging was performed with a 2-mm slice thickness and the image matrix size was 256×256 with an in-plane resolution of 51 μm. The signal decay as a function of t_d was fitted to a single exponential function for individual pixels of the image and background rates ($1/T_b$) were subtracted to obtain the spatial map of DDIF decay rates. No adjustment was made for the signal free-region outside the NMR tube. The noise level was estimated from the signal-free region and only points whose amplitudes were larger than the noise level were included in the fits. All decay curves were found to be consistent with single exponential behavior within experimental error.

To probe the interference pattern between the internal and applied field gradients ($\vec{g} = \vec{g}_{\text{ext}} + \vec{g}_{\text{int}}$), a gradient pulse of 0.5 G/cm, similar to the value of internal field gradient, was applied for 35 ms during the encoding time (t_e) periods along three different orientations (read (B_0): y, phase: x, slice: z). The corresponding decay rate was proportional to the square of the local gradient:

$$g_i^2 = g_{\text{ext}}^2 + g_{\text{int}}^2 + 2\vec{g}_{\text{ext}} \cdot \vec{g}_{\text{int}}, \tag{2}$$

where $i = 1, 2, 3$ represents three experiments with different directions of applied gradient pulses. For example, the first experiment ($i = 1$) used the PFG along the z-direction, the second experiment along y and third along x, as shown in, Fig. 4. Since the internal field gradient is only in the x–y plane due to the cylindrical symmetry of the sample, the following relations hold

$$g_1^2 = g_z^2 + g_{\text{int}}^2, \tag{3}$$

$$g_2^2 = g_y^2 + g_{\text{int}}^2 + 2\vec{g}_y \cdot \vec{g}_{\text{int}}, \tag{4}$$

$$g_3^2 = g_x^2 + g_{\text{int}}^2 + 2\vec{g}_x \cdot \vec{g}_{\text{int}}, \tag{5}$$

since the magnitude of the applied gradients was the same, the cross-terms $\vec{g}_{\text{ext}} \cdot \vec{g}_{\text{int}}$ could be obtained by subtracting g_1^2 from g_2^2 and g_3^2. In addition, the contributions from bulk T_1 and unbalanced slice gradients were removed by this subtraction. Again, single exponential fitting was performed to obtain the decay rates of individual voxels, and thus the strength of the total gradients was determined from the spatially resolved interference pattern.

The numerical calculation of the internal field was performed as follows. First, a black and white representation (1024×1024 voxels) of cylinders was created from the measured spin density image at $t_d = 50$ ms to obtain a high resolution replica of the experimental setup. To minimize the boundary effect, the image was placed at the center of a 2048×2048 area. The induced (demagnetization) field along the external field direction was calculated in the Fourier space by superposition of the dipole field from each voxel of the solid taken as a point source, valid to first order in $\triangle\chi/\chi \ll 1$ [30,31]. From this, we obtained the strength of the gradient via $g_{\text{int}} = \sqrt{(dB_y/dy)^2 + (dB_y/dx)^2}$ as well as the angle-resolved gradient $\vec{g}_{\text{int}} \cdot \hat{n}$ ($\hat{n}$ is the unit vector along the direction of applied external gradient) evaluated on the grid.

3. Experimental results and discussion

Fig. 2 shows the images at four diffusion times. Distinct decay behaviors are apparent depending on the local packing geometry. Representative packings, such as rectangular, triangular and pentagonal, are illustrated in (d) for comparison. For example, signal decay is always slower at the centers of the local packing geometry where local minima in the internal fields (and therefore minimal gradients) tend to occur. The gradual thickening of the apparent capillary walls indicates higher gradients near the walls. Such